30 GHz Surface Acoustic Wave Transducers with Extremely High Mass Sensitivity

Jiangpo Zheng[1,#], Jian zhou[1,#,*], Pei Zeng[1], Yi Liu[2], Yiping Shen[2], Wenze Yao[3], Zhe Chen[1], Jianhui Wu[1], Shuo Xiong[1], Yiqin Chen[1], Xianglong Shi[4], Jie Liu[3], Yongqing Fu[5], Huigao Duan[1,*]

[1]State Key Laboratory of Advanced Design and Manufacturing for Vehicle Body, College of Mechanical and Vehicle Engineering, Hunan University, Changsha 410082, China
[2] Hunan Provincial Key Laboratory of Health Maintenance for Mechanical Equipment, Hunan University of Science and Technology, Xiangtan 411201, China
[3] College of Electrical and Information Engineering, Hunan University, Changsha 410082, China
[4] Beijing Aerospace Micro-electronics Technology Co., Beijing 100854, People's Republic of China
[5]Faculty of Engineering and Environment, Northumbria University, Newcastle upon Tyne, NE1 8ST, United Kingdom

[#] These authors contribute equally to this work.
*Corresponding Email: jianzhou@hnu.edu.cn, duanhg@hnu.edu.cn

Abstract: A nano-patterning process is reported in this paper, which can achieve surface acoustic wave (SAW) devices with an extremely high frequency and a super-high mass sensitivity. An integrated lift-off process with ion beam milling is used to minimize short-circuiting problem and improve quality of nanoscale interdigital transducers (IDTs). A specifically designed PEC algorithm is applied to mitigate proximity effects occurring in the conventional electron-beam lithography process. The IDTs with a period of 160 nm and a finger width of 35 nm are achieved, enabling a frequency of ~30 GHz on lithium niobate based SAW devices. Both centrosymmetric type and axisymmetric type IDT structures are fabricated and results show that the centrosymmetric type tends to excite lower-order Rayleigh waves, and the axisymmetric type tends to excite higher-order wave modes. A super-high mass sensitivity of ~388.2 MHz×mm^2/μg is demonstrated, which is ~10^9 times larger than that of a conventional quartz crystal balance and ~50 times higher than a conventional SAW device with a wavelength of 4 μm.

Surface acoustic wave (SAW) devices have wide-range applications including quantum communication[1], filters in radio-frequency communication[2], micro-sensors[3] for detecting physical parameters and biochemical substances[4], microfluidics and lab-on-a-chips[5]. For most SAW applications, there is a strong demand for super-high frequency devices, for example, to enhance processing speed for significantly increased volume of information in data transmission systems[6], to reach the quantum regime[7], or to improve the sensitivity of sensor.

For sensing applications, sensitivity[8] of SAW devices is proportional to the square of their resonance frequency. The resonant frequency (f) of a SAW device follows the formula $f=v/\lambda$, where v is the velocity of a SAW mode and λ is the IDT period (or wavelength). To increase the frequency, two approaches are generally applied: 1) reducing the value of λ *via* improved patterning resolution; and 2)

exploiting slow-on-fast structures using substrates with high acoustic wave velocity, such as ZnO/SiC[9], ZnO/diamond[10], AlN/diamond[11] and AlScN/diamond[12,13]. For example, in 2012, Büyükköse *et al.* demonstrated ultra-high frequency (16.1 GHz) SAW devices on ZnO/SiO_2/Si substrate using a nanoimprint lithography[14]. In 2016, Mohammad *et al.* fabricated 14 GHz SAW devices on lithium niobate using high-resolution electron-beam lithography (EBL)[15]. In 2017 and 2018, we have achieved high frequencies of 17.7 GHz[16] and 33.7 GHz[12] on the AlN/diamond/Si and AlScN/diamond/Si substrate using EBL, respectively.

However, all the above-mentioned studies fabricated SAW devices with wavelengths larger than 200 nm. It is a great challenge to further reduce the wavelength of SAW device below 200 nm due to the fabrication difficulties. As the SAW IDT fingers are highly dense and their numbers are up to tens or hundreds of pairs, the conventionally used photolithography and lift-off processes often have the intrinsic problems of short-circuiting of IDTs. Such a problem becomes severe when the wavelength of SAW device is decreased below 200 nm. Whereas for the EBL method, the proximity effect caused by the electron beam scattering causes a relatively large dose in the middle of exposure area and a smaller dose in the surrounding area. This leads to a non-uniform dose distribution in the designed IDT pattern, which significantly degrade the quality of the IDTs and thus deteriorate the performance of SAW devices.

In this work, we integrate a specifically designed proximity-effect-correction (PEC) algorithm and a pattern transfer strategy into the conventional EBL-based patterning process. The process involves a dry lift-off process based on ion beam milling, which is able to minimize the short-circuiting problem commonly observed in the wet lift-off process, and thus significantly improves the success rate of nano-scale IDTs. The PEC algorithm obtained using the empirical formula is applied to mitigate the proximity effect in the EBL process. Nanoscale IDTs with a period (λ) of 160 nm and a finger width of 35 nm are achieved, and a frequency of 30 GHz on lithium niobate ($LiNbO_3$) based SAW devices is obtained. Finally, a super-high mass sensitivity of ~388.2 MHz×mm^2/μg has been demonstrated using the fabricated SAW device, which is ~10^9 times higher than that of a conventional quartz crystal microbalance (QCM) and ~50 times higher than that of a conventional SAW devices with a wavelength of 4 μm.

Figure 1 shows the overall structure of SAW devices in this work. The inset figures are the enlarged IDTs, two different IDT structure designs (e.g., axisymmetric-type (or AS-type) of IDTs and centrosymmetric-type (or CS-type) of IDTs) and a schematic illustration of mass loading for super-high frequency SAW sensing, respectively. The number of IDT pairs (N) for all SAW devices is 80, and the number of reflectors (N_r) is 50. The wavelength (λ) is determined by the IDT periodicity, λ=2(a+b), where a and b are the finger width and spacing, respectively. In this study, different wavelengths of 160, 200, 320, 400, 600, and 800 nm have been designed. For all the SAW devices, the aperture (L), the distance between the IDTs and reflectors (L_{rt}), and the spacing between both IDTs (L_{tt}) are 20λ, 0.75λ and 4.75λ, respectively.

In a common fabrication process, the proximity effect of electron beams causes a relatively large dose in the middle of exposure area and a smaller dose in the surrounding area, as indicated in Figs. 1(b) and 1(c), thus resulting in non-uniform dose distribution for the IDTs and subsequently leading to the failure of IDT fabrication. In this study, we proposed a specific and effective dose optimization algorithm to solve the dose non-uniformity problem during the EBL process and the dose distribution after applying the PEC algorithm is indicated in Figure 1(d). The PEC algorithm was based on the

empirical formula specifically developed for dense periodic IDTs and is more straightforward compared to the commercial software. All detailed information of the optimization algorithm is provided in the supplementary materials.

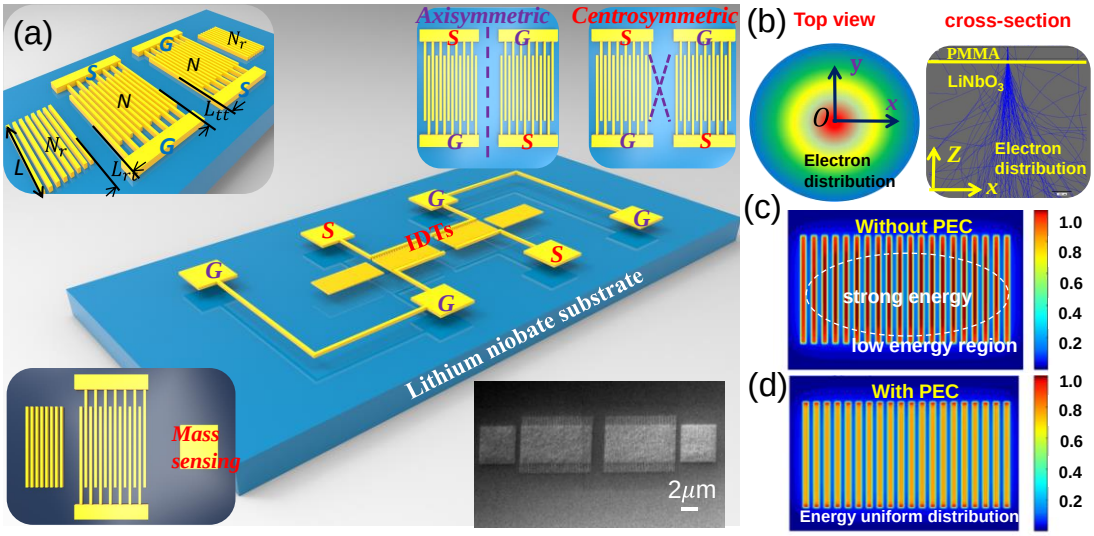

Figure 1. (a) Two-port SAW device design with Ground-Signal-Ground (GSG) electrode configuration, and the upper left, upper right, lower left and lower right of the inset figures are the magnified IDTs and reflectors structure with relevant labels, the IDT pattern of the AS-type and CS-type design, the layout of mass loading and the SEM picture of IDT pattern, respectively; (b) top view and cross-section view of electron energy distribution into the PMMA/$LiNbO_3$; (c) Uneven dose distribution of exposed IDT pattern without PEC; (d) Uniform dose distribution of exposed IDT pattern with PEC.

To avoid the short-circuiting problem in the conventional photolithography and lift-off process, we proposed a dry lift-off process based on ion beam milling, which can significantly improve the success rate of nanoscale IDT fabrication. Figure 2 shows the process flow using the EBL and ion beam milling processes. A 60 nm thick polymethyl methacrylate (PMMA) was spin-coated onto the $LiNbO_3$ substrates, which was then baked at 180°C for 5 minutes. A thin conductive polymer layer (AR-PC 5090.02, Allresist, Germany) was spin-coated on top of the PMMA for charge dissipation. After exposure, the conductive polymer was rinsed by deionized water, and then the patterns were developed in a developer solution followed by immersing the sample inside isopropanol. After evaporating the metal onto the substrate, a 100 nm thick hydrogen silsesquioxane (HSQ) layer was spin-coated onto the samples to flatten the sample surface. Subsequently, an ion beam etching process (LJK-150, Jizhixing Corp., China) was carried out to obtain the IDTs by removing the unwanted HSQ, gold and PMMA. The remaining PMMA was stripped via acetone washing and oxygen plasma. After the fabrication of SAW IDTs, the bus bar and wire pad were fabricated using the conventional photolithography and lift-off processes. Fig. 2(h) shows the differences of patterns using the conventional EBL method and our newly developed process. Clearly the latter effectively avoids the short-circuiting issues. The detailed process of device preparation is provided in the supplementary materials.

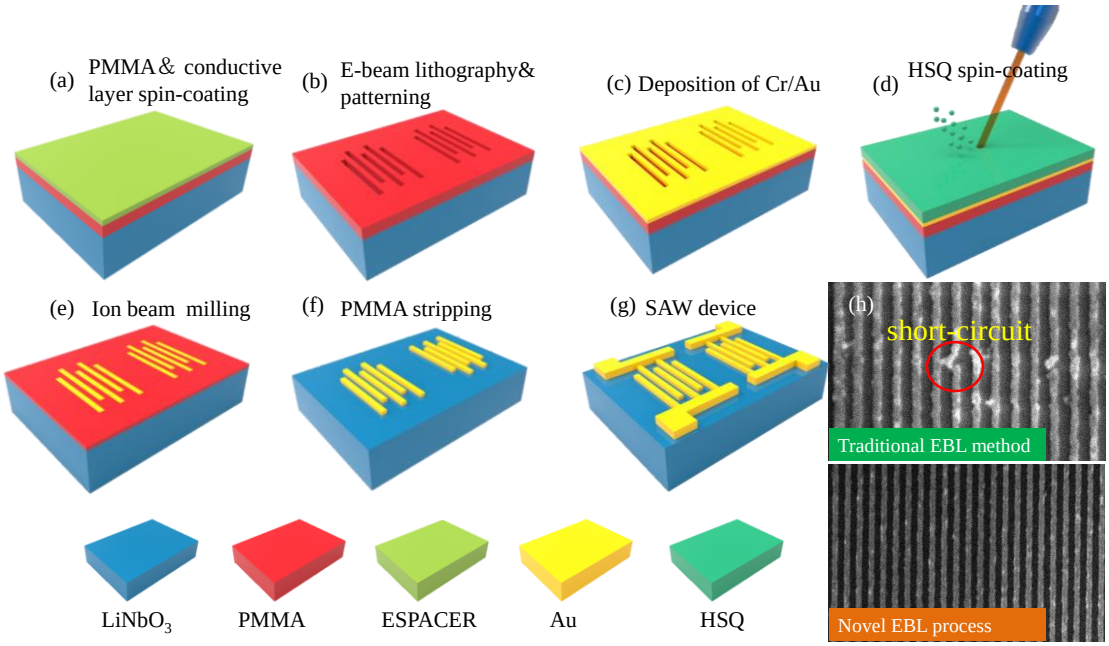

Figure 2. Schematic illustration of fabrication process for SAW devices on $LiNbO_3$. (a) Spin coating of PMMA photoresist and conductive layer; (b) EBL and development; (c) Cr/Au metallization;(d) HSQ spin-coating to flatten the surface; (e) ion-beam milling to remove unwanted gold; (f) PMMA stripping to form IDTs; (g) fabrication of bus bar and wire pad to from SAW device; (h) Comparison of typical IDT features with a wavelength of xxx nm fabricated by conventional EBL method (top) and the improved EBL process in this work (bottom).

The fabricated structures were characterized using a field-emission scanning electron microscope (FESEM, Carl-Zeiss Sigma HD). Frequency responses of the fabricated SAW devices were measured using an Agilent N5247A network analyzer. For mass sensing tests, we used the one-port resonator as shown in Fig. 1(a). We firstly fabricated the one-port SAW resonator. Then the rectangular Au pads, with a thickness of 30 nm and an area of 10 $\lambda \times 10\ \lambda$, was deposited in front of the IDTs. The distance between the mass loading area and the IDTs was 10 λ.

Figure 3 shows SEM images of the fabricated SAW IDTs with different wavelengths from 800 nm to 160 nm. It can be clearly seen that our process is effective to fabricate nanoscale wavelengths of SAW devices. An ultra-high resolution with Au linewidth of ~35 nm (inset Fig. 3(f)) and a wavelength of 160 nm was achieved, corresponding to a ~45% metallization ratio. As far as we know, 160 nm represents the smallest wavelength for all the reported SAW devices in literature so far.

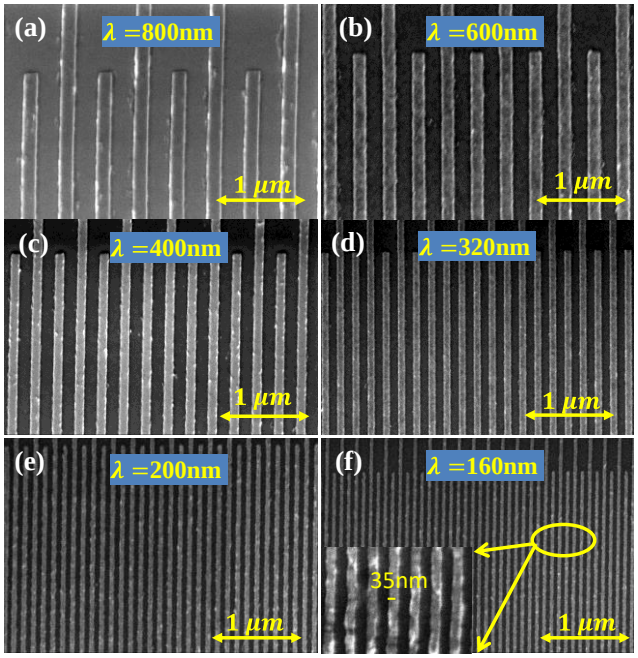

Figure 3. FESEM images of SAW IDTs of various wavelengths: (a) 800 nm, (b) 600 nm, (c) 400 nm, (d) 320 nm, (e) 200 nm, and (f) 160 nm.

Figure 4(a) shows the reflectance (S_{11}) signals of AS-type and CS-type SAW devices with different wavelengths and a fixed IDT thickness of 18 nm. Results showed that all of the SAW devices with different wavelengths present multiple wave modes for both AS-type and CS-type structures. Simulations based on the commercial COMSOL Multiphysics software verify that the obtained wave modes correspond to shear-horizontal (SH) type wave, Rayleigh-wave type SAWs, Longitudinal leaky SAWs (LLSAWs), and longitudinal bulk wave(LW), respectively, which are consistent with the results obtained from the conventional SAW devices[17]. The simulated particle vibration modes are shown in the inset of Fig. 4(a). When the wavelength was decreased from 800 nm to 160 nm, the frequency was gradually increased from the range of 4~10 GHz to the range of 15~30 GHz, whereas the insertion loss and signal amplitude were found to decrease slightly. The reason for this decreased insertion loss and signal amplitude for the smaller wavelength devices may be due to the larger impedance of the IDTs with very narrow and slender IDT fingers. For smaller wavelength features, it is more difficult to achieve uniform width of IDTs, thus leading to weaker signals.

Nevertheless, the SAW device with the CS-type design and a wavelength of 160 nm achieved a high resonant frequency of ~30 GHz, which is the highest reported frequency of SAW device on lithium niobate substrate as far as we have searched in literature. To verify that this ~30 GHz frequency is truly excited by the SAW but not due to the noise/parasitic waves, we conducted a theoretical analysis of the SAW device with the wavelength λ of 160 nm using the finite element model/boundary element model (FEM/BEM). The detailed theoretical analysis procedures can be referred to our previous work[18]. Figure 4(b) shows the obtained analysis results, which indicates a good agreement with the experimental results. It should also be noted that when the wavelength is less than 400 nm for the AS-type devices, the shear horizontal wave (SH mode) shows a lower frequency value than that of the Rayleigh wave. This is mainly caused by the relatively thick electrode used for the devices with such small wavelength[19].

Comparing the results of AS-type SAW devices with those of CS-type SAW devices, the CS-type devices generally have higher frequency values and better device performance (e.g., larger signal amplitudes) for the Rayleigh wave mode (R_0). However, for the higher order LLSAW modes, their signal amplitudes of the CS-type modes are smaller than those of the AS-type ones.

The electromechanical coupling coefficient (k^2_{eff}) of the SAW devices can be obtained using the following formula[9]:

$$k^2_{eff} = \frac{\pi}{2} \times \frac{f_s}{f_p} \times \tan\left(\frac{\pi}{2} \times \frac{f_p - f_s}{f_p}\right) \quad (6)$$

where f_p and f_s refer to parallel and series frequencies, respectively. The obtained results shown in Fig. 4(c) indicate that as the wavelength is gradually decreased from 800 nm to 160 nm, the k^2_{eff} values of the Rayleigh waves (R_0) of the CS-type devices are decreased whereas those of the AS-type ones are increased.

The dispersion relation between the phase velocities and the wavelength of the SAW is shown in Fig. 4(d). With the wavelength decreased from 800 nm to 160 nm, the obtained wave velocities of the Rayleigh wave modes, LLSAWs and SH wave are decreased with the decrease of the wavelength. The reason for the decreased velocity of acoustic wave modes is because there is more significant mass-loading effect for the device with smaller wavelength on the same substrate.

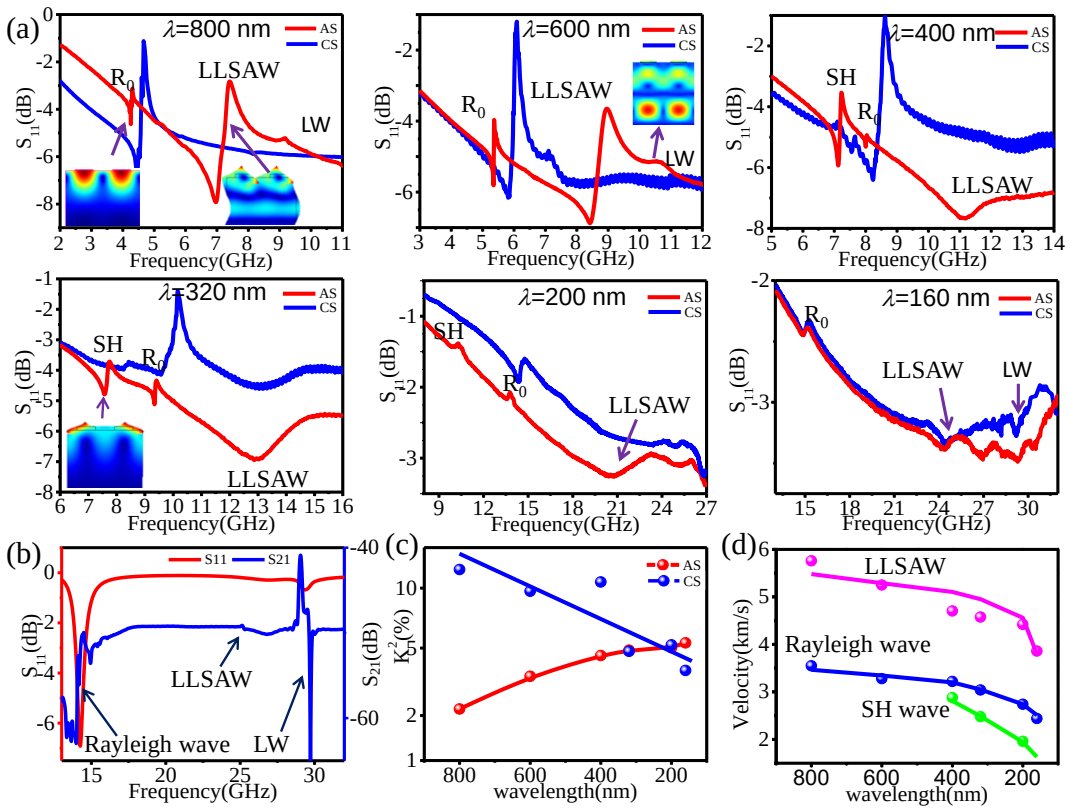

Figure 4. (a) S_{11} parameters for both AS-type and CS-type devices with different wavelengths decreasing from 800 nm to 160 nm. The insets give the COMSOL simulated z-displacement field plots of Rayleigh modes and harmonic order modes. (b) Theoretical calculation result of 160 nm period device. (c) The electromechanical coupling factor of AS-type and CS-type devices. (d) Dispersion relation between the phase velocities of different Rayleigh modes and different wavelength. Lines are simulated results and symbols are experimentally determined values.

Figure 5 shows mass sensing results using the super-high frequency device with wavelengths of 400 nm and 200 nm. For the device with a wavelength of 400 nm, the resonant frequencies of the SAW device without any mass loading are 7.860 GHz and 12.032 GHz, whereas the frequency values are decreased to 7.820 GHz and 11.807 GHz with the mass loading on the SAW devices, respectively. Similarly, the frequency of the device with the wavelength of 200 nm is shifted from 14.175 GHz to 14.043 GHz.

The mass sensitivity of the SAW device can be defined as the changes of frequency shift due to the mass change in a given area of A, $(\Delta f/\Delta m/A)$[20], in which Δm is the change of mass loading and A is the area of the sensing region. For the SAW device with a wavelength of 400 nm, the sensitivity values for the Rayleigh and LLSAWs mode are estimated to be 69.013 MHz×mm^2/μg and 388.199 MHz×mm^2/μg, respectively. The Rayleigh mode sensitivity of the device with a 200 nm wavelength is approximately 221.171 MHz×mm^2/μg. The above results clearly show that for the Rayleigh mode, the device with a smaller wavelength will have a larger mass sensitivity due to its higher resonant frequency. The higher-order mode (LLSAWs) has a larger sensitivity compared with that of the Rayleigh wave mode. The highest sensitivity of 388.199 MHz×mm^2/μg achieved in in this study is ~10^9 times larger than that of a conventional QCM device[21] and ~50 times larger than that of a conventional SAW device with a frequency of 978 MHz[22], which have been listed in Table 1.

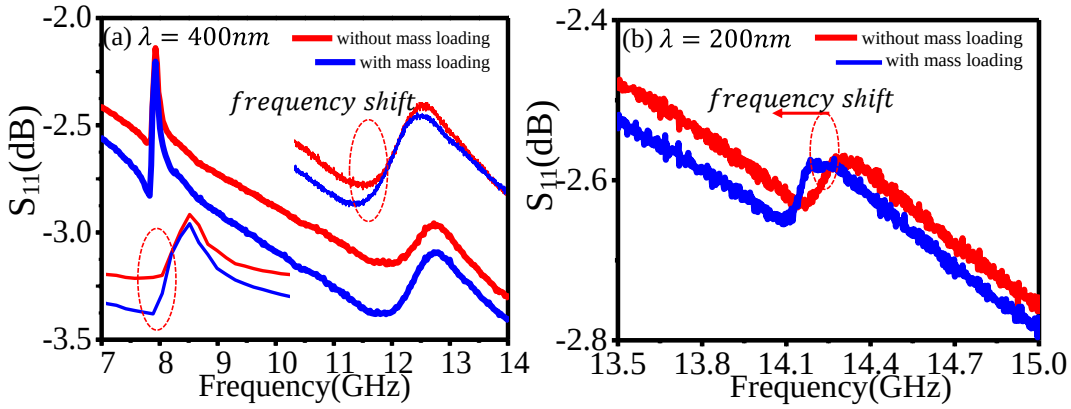

Figure 5. Frequency response for the SAW device with or without mass loading with the wavelength of (a) 400 nm and (b) 200 nm, showing the frequency shift for mass sensing.

TABLE 1. Characteristics of mass sensitivity SAW and QCM

Reference	***Year***	***Type***	***Resonant frequency(GHz)***	***Sensitive of Mass sensing***
[22]	2010	SAW sensor	0.978	8.23 MHz×mm^2/μg
[23]	2015	SAW sensor	0.124	2.51 MHz× mm^2/μg
[24]	2016	SAW sensor	0.262	275 MHz/μg
[25]	2017	SAW sensor	0.44	40.2 KHz/μg
[26]	2013	QCM	0.008	714 Hz/μg
[27]	2017	QCM	0.01	1573 Hz/μg
[28]	2019	QCM	0.008	727 Hz/μg
This work	2019	SAW sensor	14.073	388.199 MHz×mm^2/μg(24.26×10^{3}GHz/μg)

In conclusion, super-high frequency SAW devices up to 30 GHz on lithium niobate substrate were successfully fabricated using a newly proposed EBL process. The process was achieved by integrating a dry lift-off process with the ion beam milling, which can minimize the short-circuiting problem occurring in the conventional photolithography and lift-off process and thus significantly improve the success rate of nanoscale IDTs fabrication. Meanwhile, a specific algorithm for IDTs fabrication was developed to mitigate the proximity effect occurring in the EBL process, with which extremely narrow nano-IDTs with 35 nm finger width were obtained. Super-high sensitivity for mass sensing was achieved with a sensitivity of 388.199 MHz×mm^2/μg, which is ~10^9 times larger than that of the conventional QCM and ~50 times larger than that of a conventional SAW devices with a wavelength of 4 μm. The demonstrated ultra-high frequency $LiNbO_3$-based SAW devices have great potentials for applications in quantum acoustic devices, nonlinear acoustic devices and high-frequency filters.

See supplementary material for the detailed micro-fabrication process of high frequency SAW devices, the complete specific PEC algorithm, SEM results of dose distribution with/without PEC specific algorithm and other data of high frequency SAW devices.

This work was supported by the Key Research Project of Hunan Province (2018GK2044, 2019GK2111). The UK Engineering and Physical Sciences Research Council (EPSRC) grants EP/P018998/1, Newton Mobility Grant (IE161019) through Royal Society and the National Natural Science Foundation of China

References

[1]K. J. Satzinger, Y. Zhong, H.-S. Chang, G. A. Peairs, A. Bienfait, M.-H. Chou, A. Cleland, C. R. Conner, É. Dumur, and J. Grebel, Nature **563**, 661 (2018).

[2]S. Fu, W. Wang, L. Qian, Q. Li, Z. Lu, J. Shen, C. Song, F. Zeng, and F. Pan, IEEE Electron Device Lett. **40**, 103 (2018).

[3]J. Zhou, J. Zheng, X. Shi, Z. Chen, J. Wu, S. Xiong, J. Luo, S. Dong, H. Jin, and H. Duan, J. Electrochem. Soc. 166, B432 (2019).

[4]Y.-S. Choi, J. Lee, Y. Lee, J. Kwak, and S. S. Lee, Appl. Phys. Lett. **113**, 083702 (2018).

[5]A. Ozcelik, J. Rufo, F. Guo, Y. Y. Gu, P. Li, J. Lata, and T. J. Huang, Nat. Methods. **15**, 1021 (2018).

[6]A. Almirall, S. Oliveri, W. Daniau, S. Margueron, T. Baron, P. Boulet, S. Ballandras, S. Chamaly, and A. Bartasyte, Appl. Phys. Lett. **114**, 162905 (2019).

[7]A. Noguchi, R. Yamazaki, Y. Tabuchi, and Y. Nakamura, Phys. Rev. Lett. **119**, 180505 (2017).

[8]S. W. Wenzel and R. M. White, Appl. Phys. Lett. **54**, 1976 (1989).

[9]S. Fu, W. Wang, Q. Li, Z. Lu, Z. Chen, J. Luo, J. Shen, R. Wang, C. Song, and F. Zeng, Appl. Phys. Lett. **114**, 113504 (2019).

[10]P. Kirsch, M. B. Assouar, O. Elmazria, V. Mortet, and P. Alnot, Appl. Phys. Lett. **88**, 223504 (2006).

[11]L. X. Chen, H. Liu, S. Liu, C. M. Li, Y. C. Wang, K. An, C. Y. Hua, J. L. Liu, J. J. Wei, L. F. Hei, and F. X. Lv, Appl. Surf. Sci. **431**, 152 (2018).

[12]L. Wang, S. Chen, J. Zhang, J. Zhou, C. Yang, Y. Chen, and H. Duan, Appl. Phys. Lett. **113**, 093503 (2018).

[13]Y. Q. Fu, J. Luo, N.-T. Nguyen, A. Walton, A. J. Flewitt, X.-T. Zu, Y. Li, G. McHale, A. Matthews, and E. Iborra, Prog. Mater. Sci. **89**, 31 (2017).

[14]S. Büyükköse, B. Vratzov, D. Ataç, J. van der Veen, P. Santos, and W. G. van der Wiel,

Nanotechnology. **23**, 315303 (2012).
[15]M. A. Mohammad, X. Chen, Q. Y. Xie, B. Liu, J. Conway, H. Tian, Y. Yang, and T. L. Ren, IEEE Int. Electron Devices Meet. **15**, 495(2016).
[16]L. Wang, S. Chen, J. Zhang, D. Xiao, K. Han, X. Ning, J. Liu, Z. Chen, and J. Zhou, Appl. Phys. Lett. **111**, 253502 (2017).
[17]A. Isobe, M. Hikita, and K. Asai, IEEE Trans. Ultrason, Ferroelectr, Freq Control. **52**, 1812 (2005).
[18]J. Zhou, X. Shi, D. Xiao, X. Wu, J. Zheng, J. Luo, M. Zhuo, X. Tao, H. Jin, and S. Dong, J. Micromech. Microeng. **29**, 015006 (2018).
[19]M. Kadota, T. Yoneda, K. Fujimoto, T. Nakao, and E. Takata, IEEE Trans. Ultrason, Ferroelectr, Freq Control. **51**, 202 (2004).
[20]S. Thomas, M. Cole, F. H. Villa-Lopez, and J. W. Gardner, Sens. Actuators A. **244**, 138 (2016).
[21]W. Ma, S. Tang, Y. Wei, and G. Xie, in *Micro Nano Lett*. **12**, 113 (2017).
[22]H. C. Ou and M. Zaghloul, IEEE Electron Device Lett. **31**, 518 (2010).
[23]S. Koochakzadeh, M. Richardson, V. R. Bhethanabotla, and S. K. S. Sankaranarayanan, IEEE Sens. 855(2015).
[24]S. Thomas, M. Cole, F. H. Villa-López, and J. W. Gardner, Sens. Actuators A.**244**, 138 (2016).
[25]V. Ulianova, V. Selotkin, A. Zazerin, A. Orlov, Y. Yakimenko, and O. Bogdan, Int. Conf. Electron. Nanotechnol. 100(2017).
[26]M. Stoytcheva, R. Zlatev, S. Cosnier, M. Arredondo, and B. Valdez, Biosens. Bioelectron. **41**, 862 (2013).
[27]W. Y. Ma, S. Tang, Y. H. Wei, and G. Z. Xie, Micro Nano Lett. **12**, 113 (2017).
[28]D. Zhang, H. Chen, X. Zhou, D. Wang, Y. Jin, and S. Yu, Sens. Actuators A. **295**, 687 (2019).